Chapter 6 Sign reversal exchange bias and Magnetic structure of $CeCrO_3$

6.1 Introduction

In this chapter, we conducted an investigation into the nuclear and magnetic structure, as well as the magnetic properties, of $CeCrO_3$ nanoparticles synthesized using a one-step solution combustion method. The nuclear structure analyses from XRD and NPD showed the formation of pure distorted orthorhombic Pnma structure, and the composition analysis confirms the stoichiometry of sample, which is discussed in detail in sections 6.2. The magnetic structural analysis, obtained through the fitting of NPD data, is discussed in Section 6.3, revealing the presence of more than one magnetic structure at both low temperature (6K) and high temperature (235K). To further verify the magnetic structure at these temperatures, we performed magnetization versus temperature and magnetization versus field experiments using a specific protocol. Detailed discussions of these experiments are presented in Sections 6.3.1 and 6.3.2, respectively. The magnetization measurements support the transformation of the magnetic structure from Γ_4 to Γ_2 as the temperature decreases from 235K to 6K. In Section 6.4, we provide a summary of all the significant findings.

6.2 Structural and compositional analysis

Figure. 6.1 shows the room temperature x-ray diffraction pattern of $CeCrO_3$ sample with the Rietveld refinement using Pnma space group.

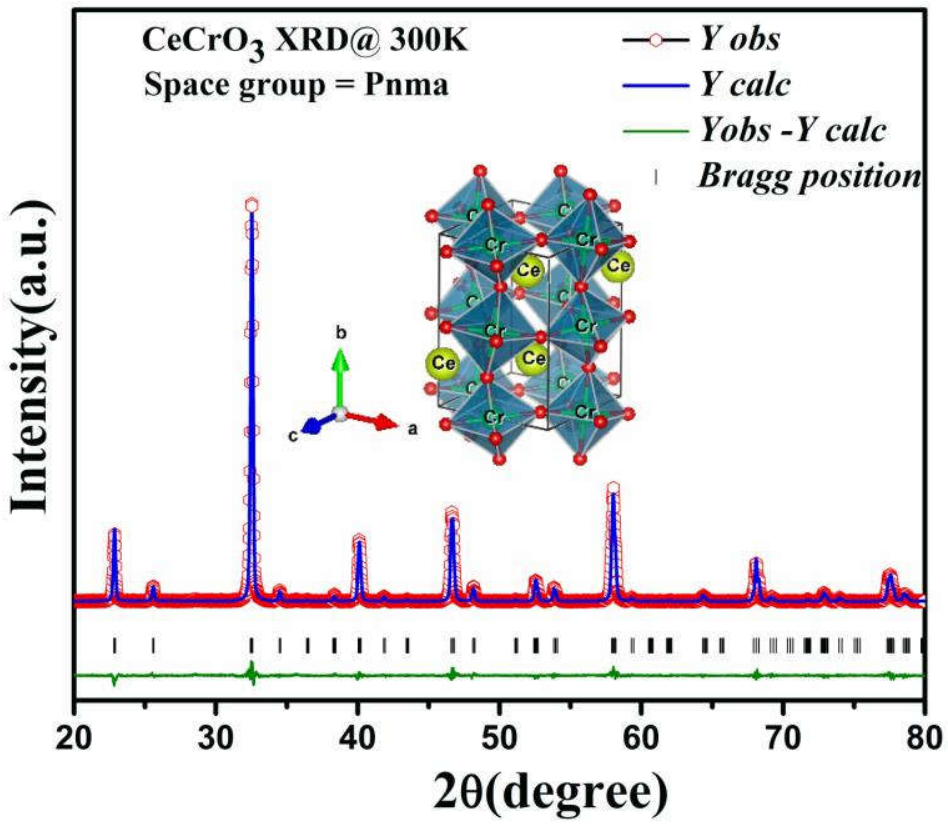

Figure 6.1 Rietveld refined room-temperature X-ray powder diffraction data of $CeCrO_3$.

Pseudo-voigt peak profile function is used for the refinement. The best fit confirms the formation of single phase orthorhombic, Pnma structure. The refinement of TOF NPD pattern at room temperature is conducted using the "T.O.F. p-Voigt * B-t-B exponential" peak profile function. The results are shown in figure 6.2. NPD Fitting confirms that the Ce, Cr, and the two oxygen atoms O1 and O2, occupy the 4*c*, 4*b*, 4*c*, and 8*d* Wyckoff positions

of the *Pnma* structure, respectively. The structural parameters obtained from refinement are shown in Table 6.1 and the crystal structure models generated from cif after refinement are depicted in the corresponding insets of Figures. 6.1 and 6.2.

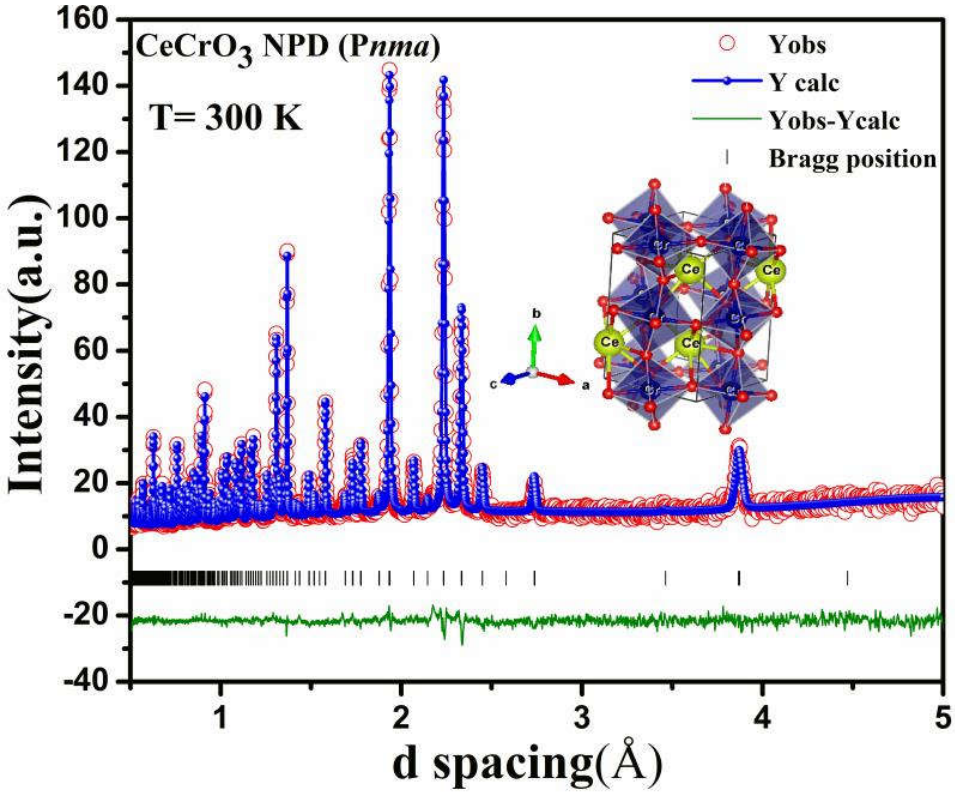

Figure 6.2: Rietveld refined room-temperature time of flight (TOF) neutron powder diffraction (NPD) data of the same $CeCrO_3$ sample.

The lattice parameters a, b, c and the unit cell volume along with bond angle are closely matched with the previous report on $CeCrO_3$ synthesized through combustion method. Apical Cr-O1 bond length and, planner Cr-O2 and Cr-O2' are found to unequal which confirms the octahedral distortion in the system. The refined parameters revel good agreement between parameters refined from our XRD and NPD patterns and previously reported data hence reliable to discuss further the temperature dependent NPD. Scanning electron microscopy (SEM) image of $CeCrO_3$ perovskite synthesized through nitrate solution

Table 6.1 Crystal structure parameters of $CeCrO_3$ obtained from the Rietveld refinement RT and low-temperature (215 and 6K) diffraction (XRD and TOF NPD) data.

Temperature **Data type**	**300K** **XRPD**	**300K** **NPD**	**215K** **NPD**	**6K** **NPD**
a	5.4743(3)	5.47377(17)	5.47077(18)	5.4686(3)
b	7.7340(3)	7.7314(2)	7.72453(17)	7.7134(2)
c	5.4802(3)	5.47925(19)	5.47604(16)	5.4742(2)
V	232.02	231.8813	231.4127	230.88
Ce				
x	0.0273(1)	0.0290(1)	0.0292(1)	0.0295(1)
y	0.25000	0.25	0.25	0.25
z	-0.0066(2)	-0.0062(3)	-0.0061(3)	-0.0064(2)
Cr/Fe				
x	0.00	0	0	0
y	0.00	0	0	0
z	0.50	0.5	0.5	0.5
O1				
x	0.4878(14)	0.4930(16)	0.4857(16)	0.4848(15)
y	0.25000	0.25	0.25	0.25
z	0.075(2)	0.075(3)	0.070(2)	0.072(2)
O2				
x	0.281(2)	0.280(3)	0.283(2)	0.286(2)
y	0.0333(14)	0.0325(14)	0.0372(12)	0.0347(12)
z	0.720(2)	0.712(2)	0.718(2)	0.719(2)
Cr(Fe)-O1-Cr(Fe)	155.69(9)	155.963	155.787	155.33
Cr(Fe)-O2-Cr(Fe)	159.5(5)	157.6	157.4	157.05
Cr(Fe)-O1	1.978(2)	1.9762(5)	1.9751(5)	1.9739(7)
Cr(Fe)-O2	1.971(11)	1.977(11)	1.9739(16)	1.977(2)
Cr(Fe)-O2’	1.964(11)	1.9707(11)	1.9729(16)	1.971(2)
<Cr-O>	1.971	1.9746	1.9740	1.9740

combustion method is shown in figure. 6.3(a). The average particles size is found to be ~50 nm. EDS analysis show 50%-50% composition of Ce and Cr (Figure. 6.3(b)). X-ray diffraction (XRD) and time of flight (TOF) neutron powder diffraction (NPD) techniques are used to determine the nuclear and magnetic structure of $CeCrO_3$ nanoparticles.

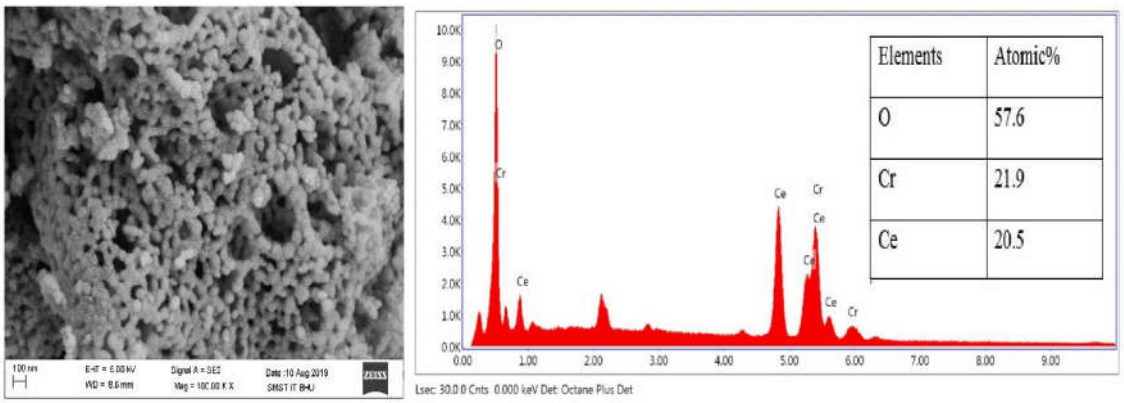

Figure 6.3 SEM and EDS spectra of $CeCrO_3$.

6.3 Low temperature neutron diffraction

The TOF neutron diffraction data of $CeCrO_3$ at various temperatures ranging from 6 K to 300 K, are shown in figure. 6.4. The refinement of RT NPD pattern with Pnma space group

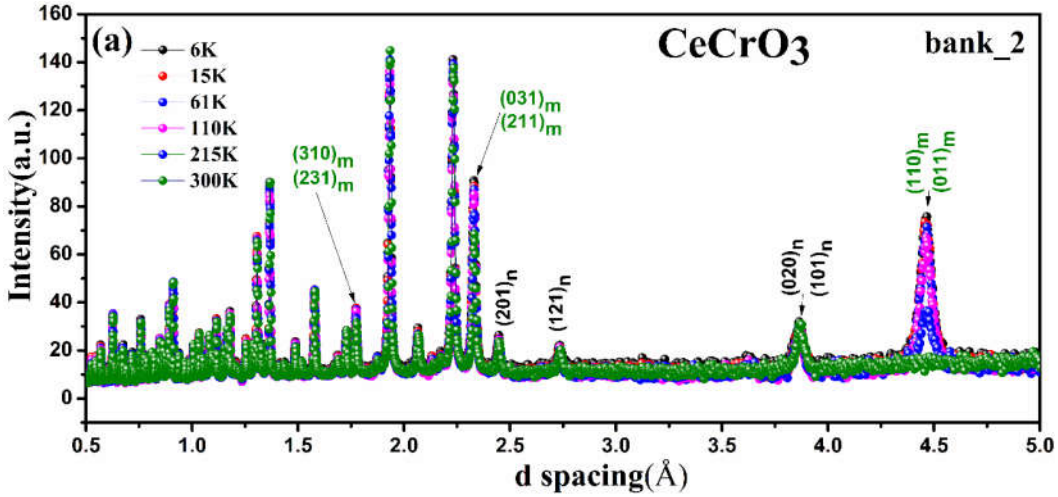

Figure 6.4 Temperature-dependent TOF-NPD data taken during warming at 6,15,61,110,215 and 300 K.

shows that except (110)/(011), all others peaks arise out of coherent nuclear scattering of neutron. The Neel temperature T_N, is reported to be 260K [91,93]. Below T_N, i.e at 215 K, a prominent magnetic scattering peak is observed at d = 4.45Å. Such additional Bragg peak confirms the long range antiferromagnetic ordering below T_N. Further, other magnetic contribution is noticed from the peaks at *d* =2.3 and 1.7 Å corresponding to the Bragg peaks (211)/(031) and (310)/(231), respectively. The intensity of these peaks also increases with decrease in temperature. In literature, (110)/(011) and (211)/(031) are also observed by Taheri et al. and Shukla et al. in $CeCrO_3$[90,91]. In addition, Shukla et al. have reported an additional Bragg peak below 100 K at *d* = 3.15 Å due to the polarization of Ce^{3+}[90] . Which, we do not observe such peaks in NPD pattern data below 100 K, similar to Taheri et al [93]. The intensity of (110)/(011) is found to increase below 215 K upto 61 K and remains unaltered with further decrease in temperature. Further, we have carried out the nuclear refinement of the low-temperature neutron diffraction patterns to determine the size of the magnetic and chemical unit cell which is found to be same. The magnetic peaks are indexed as (110) and/or (011) based on the Pnma parent unit cell basis vector, the magnetic propagation vector, k is (0,0,0). The occurrence of various possible spin configurations for k= (0,0,0), the magnetic ordering for a Pnma structure is well studied and successfully applied on rare earth orthochromites [93]. For k= (0,0,0) there are eight possible spin configurations of a Pnma structure with magnetic ions at 4b and 4c site. From the eight possible irreps, only four irreps such as Γ_1, Γ_2, Γ_3, and Γ_4 are allowed for the finite ordered moment of a transition metal magnetic ion at the 4*b* site. The other four Γ_5, Γ_6, Γ_7, and Γ_8 are allowed at the 4*c* site for rare earth magnetic ion. The spin configurations of Cr^{3+} and Ce^{3+} magnetic ions are determined through combined nuclear and magnetic structure refinement

using Full-Prof. The Bilbao crystallography server is used to generate magnetic structure crystal information files (MCIFs) with desired superimposition of more than one irreps. for magnetic Rietveld refinement, out of the eight possible spin configurations, only those have a finite moment atthe 4*b* site (Cr^{3+}) are selected, i.e., *Pnma*:$\Gamma_1(A_x,G_y,C_Z;C_z^R)$, *Pn'm'a*:$\Gamma_2(F_x,C_y,G_Z;\ F_x^R,\ C_y^R)$, *Pnm'a'*:$\Gamma_3(C_x,F_y,A_Z;C_x^R,\ F_y^R)$, and *Pn'ma'*: $\Gamma_4(G_x,A_y,F_Z;\ F_Z^R)$ [123]. During the refinement, all the components of the selected irreps are set free. Considering the contribution of Ce^{3+}along with the magnetic ion with Cr^{3+}, the fitting shows no significant improvement in goodness of fit parameters. Since rare earth ions show ordering at low temperature, it is quite unphysical to consider Ce^{3+} ordering at high temperature i.e at 215 K. Therefore, the observed magnetic ordering totally arises due to Cr^{3+} only (Cr^{3+}-O-Cr^{3+}). Such magnetic ordering of Cr^{3+} below T_N are canted in nature and it gives rise to the weak ferromagnetic moment due to Dzyaloshinskii–Moriya interaction [123]**.** The NPD data obtained at 215 K demonstrates a nearly identical fitting pattern with the magnetic structures Γ_4, Γ_2, and Γ_1. Similarly, at temperature 6 K, the NPD data also exhibits a comparable fitting pattern with the magnetic structures Γ_4, Γ_2, and Γ_1(figure 6.5). Due to the minimal disparity in the lattice parameters, a and c, as well as the strong coupling between the magnetic moments along (110) and (011) directions, it becomes challenging to ascertain the exact magnetic configurations based solely on the fitting results. In literature, Shukla et al. have reported Γ_4 magnetic structure in $CeCrO_3$inthe temperature range of 22-260 K excluding the additional Bragg peak below 100K. It is known that the magnetic structure transformation from Γ_4 to Γ_2 or Γ_1 in $RCrO_3$ with magnetic rare earth ion which occurs due to either the polarization of rare earth ion due to Cr^{3+} or due to weak rare earth ordering [123]. In this context, Cao et al. report spin reorientation transition from Γ_4 to Γ_2 when temperature decreases from

16K to 6K. In this case, we have carried out few magnetic measurements to ascertain the Γ_4 to Γ_2 magnetic structural transformation in these $CeCrO_3$ nanoparticles.

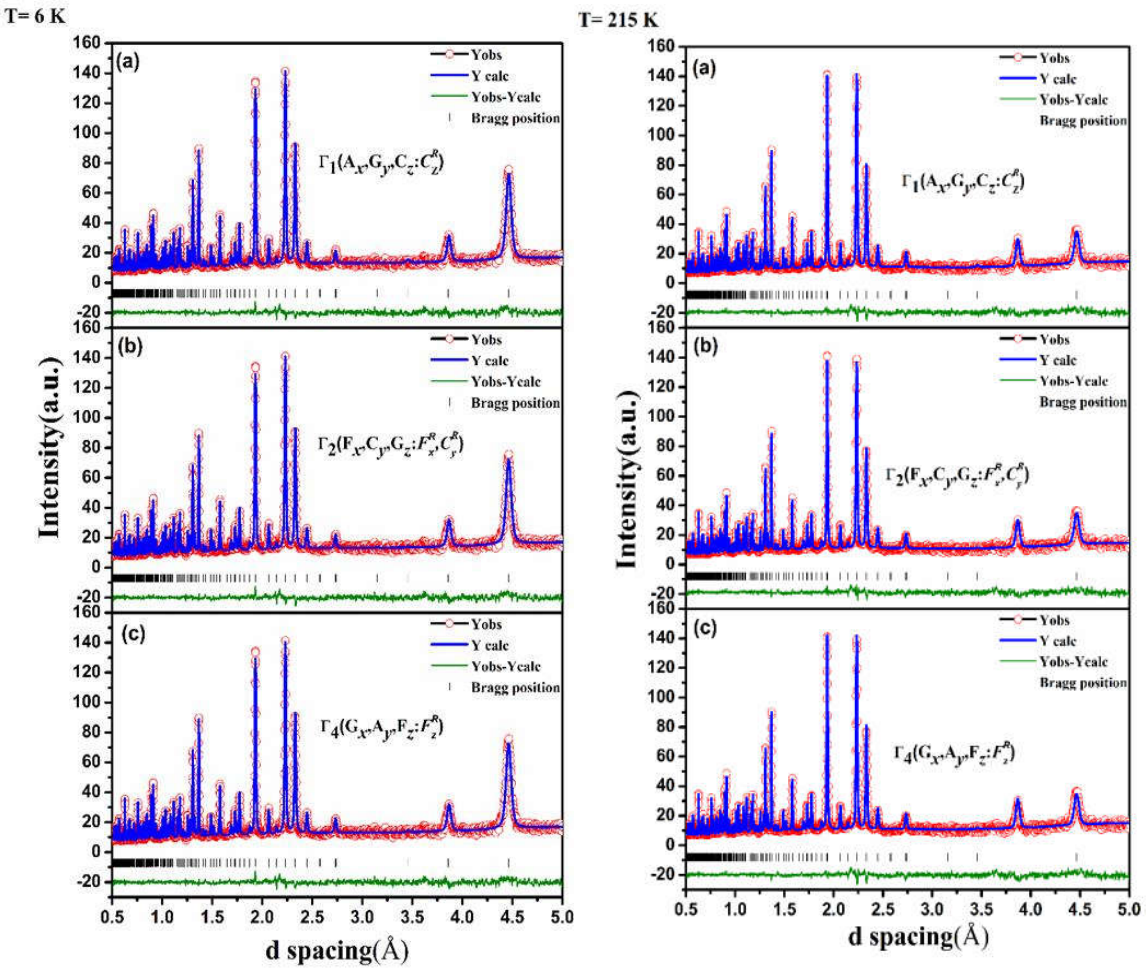

Figure 6.5 (a), (b), (c) Rietveld refined TOF NPD patterns collected at 6 K and 215K showing the typical fit quality of the refinement based on Γ_1, Γ_2, and Γ_4 irreps in respectively.

6.4 Magnetic properties

6.4.1 Temperature dependent magnetization

Temperature dependent magnetization under ZFC (zero field cooled) and FCW (field cooled warming) of $CeCrO_3$ at 0.5 kOe external applied magnetic field are shown in figure. 6.6(a).

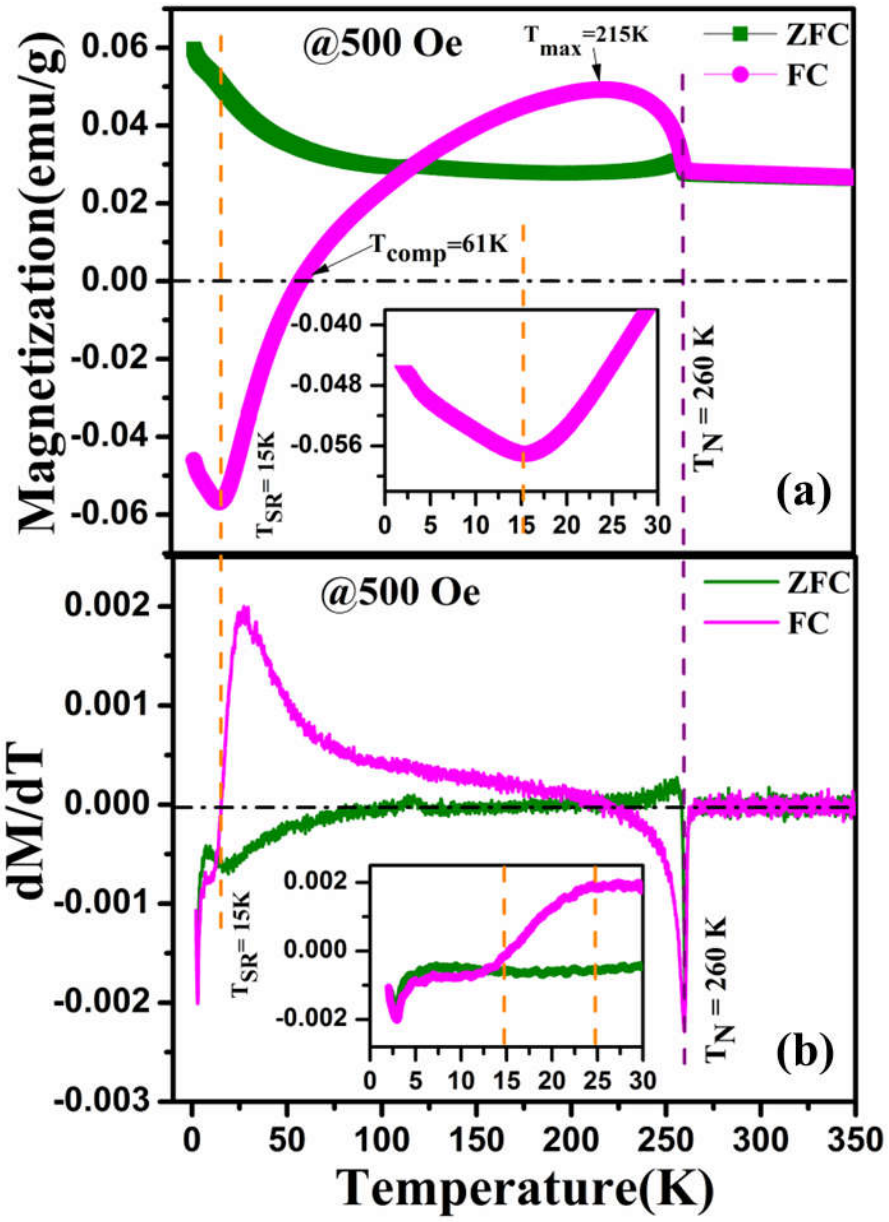

Figure 6.6 (a)Zero-field cool (ZFC) and field-cooled warming (FCW) dc-magnetization data of $CeCrO_3$ measured under 500 Oe. (b) The corresponding first-derivative (dM/dT) curves.

Magnetization curve recorded under ZFC and FCW mode shows a paramagnetic to antiferromagnetic transition at 260 K, T_N which is consistent with the T_N reported for both bulk and nano-particles of $CeCrO_3$ [85,91]. The T_N is due to the ordering of Cr^{3+}moments at 260K. Below T_N, field cooled magnetization (M_{FC}) increases showing a maximum

magnetization ~0.049 emu/g at ~215K (T_{max}). Such increase in magnetization arising due to the canted antiferromagnetic ordering of Cr^{3+}moment results into a weak ferromagnetic component in the field direction. With further decreasing the temperature, M_{FC} decreases and crosses the zero magnetization axis at a temperature known as compensation temperature (T_{comp}), observed at 58K. The decrease in M_{FC} is attributed to the canted antiferromagnetic ordering of Cr^{3+}moments which imposes a local field upon the neighboring Ce^{3+}moments. Hence, the Ce^{3+}moments experience a net local field, which is the superposition of the internal field due to the Cr^{3+}moments and the applied external field. The resultant antiferromagnetic coupling between Ce^{3+} and the canted Cr^{3+}moments polarizes the Ce^{3+}moments antiparallel to the weak ferromagnetic component of the canted Cr^{3+}moment. With further decrease in the temperature, the competition between Cr^{3+} and Ce^{3+} moments result in the compensation of the net magnetization which is observed at 58 K, T_{comp}. Below T_{comp}, a negative magnetization is observed which approaches a maximum magnitude of 0.056 emu/g ata temperature known as spin reorientation transition, T_{SR} observed at 15 K followed by an increase in magnetization down to 2 K. Inset of figure 6.6(a) depicts the enlarged view of T_{SR}. On the other hand, M_{ZFC} remains positive in whole temperature range of 2-350 K. Below T_N, M_{ZFC} shows a maximum at 260 K and remains unchanged down to 110K. Further with decrease in temperature, M_{ZFC} increases down to 2K followed by a change in slope at 20K. Such change in slope corroborates with the T_{SR} and is attributed to the ordering of Ce^{3+}as reported previously [85]. Similar magnetization under ZFC has been observed in $GdCrO_3$ around T_{SR} [124]. The first derivative of M_{ZFC} and M_{FCW} vs. temperature are shown in figure 6.6(b). Negative kink in dM/dT at 260 K further confirms the T_N. Below T_N, a maxima at 30K in FC accompanied with minima in ZFC at 20K is observed. Thereafter,

at around 15 K both the curves crosses each other, which indicating the rotation of Cr^{3+} moment to a new spin configuration between 30 K to 15K. Similar kind of rotation have been previously reported in $GdCrO_3$ and $SmCrO_3$[124,125]. The susceptibility of $CeCrO_3$ in ZFC, FCW, and FCC modes are found to be same to that of $GdCrO_3$, $TmCrO_3$, and $YbCrO_3$ [48,58,75,124–127]. In these systems, negative magnetizations are well explained by the rotation of rare earths in the internal magnetic field generated from the canted Cr^{3+} ferromagnetic component. $GdCrO_3$ exhibit a canted antiferromagnetic ordering of Cr^{3+} of the Γ_4 type just below T_N, which transform to Γ_2 type antiferromagnetic ordering at low temperature due to the rotation of Cr^{3+} in ac plane [124]. Similarly canted antiferromagnetic ordering of Cr^{3+} has also been reported in $YbCrO_3$ and $TmCrO_3$ [126,127]. Therefore, we believe that the $CeCrO_3$ also exhibits a canted G_z type antiferromagnetic ordering of Cr^{3+}. For better understanding of change in spin configuration, we have performed a number of temperature dependent magnetization measurements under FCC and FCW at 0.5 kOe external magnetic field. FCC/FCW magnetization vs. temperature measurement carried out from 350 K down to 70, 45, 30, 15,10 K, and are shown as figure. 6.7. It is evident from measurement that the temperature dependent magnetization is reversible for 70, 45 and 30 K. However, the plot at 15 and 10K shown as in inset of figure. 6.7 clearly demonstrates the irreversibility in M_{FCC} and M_{FCW}. Below 30 K, i.e. at 15 K, the M vs. T becomes irreversible. While complete reversibility in FCC and FCW within temperature range 30 K-350 K suggest continuous rotation of Cr^{3+}, irreversibility in FCC and FCW below 30K could indicate the transformation of Cr^{3+} from one spin configuration to another. Such kind of irreversibility demonstrated in $SmCrO_3$ around T_{SR}, confirms the polarization of spin configuration of Cr^{3+} from Γ_4 to Γ_2 below 30 K [125]. Although NPD analysis suggests the possibility of Γ_4 at high

temperature and Γ_4 and/Γ_2 at low temperature, the reversibility in M_{FCC} and M_{FCW} below 30K rules out the Γ_4. Thus we confirm that the Γ_4 magnetic structure transform to Γ_2 below 30 K in $CeCrO_3$.

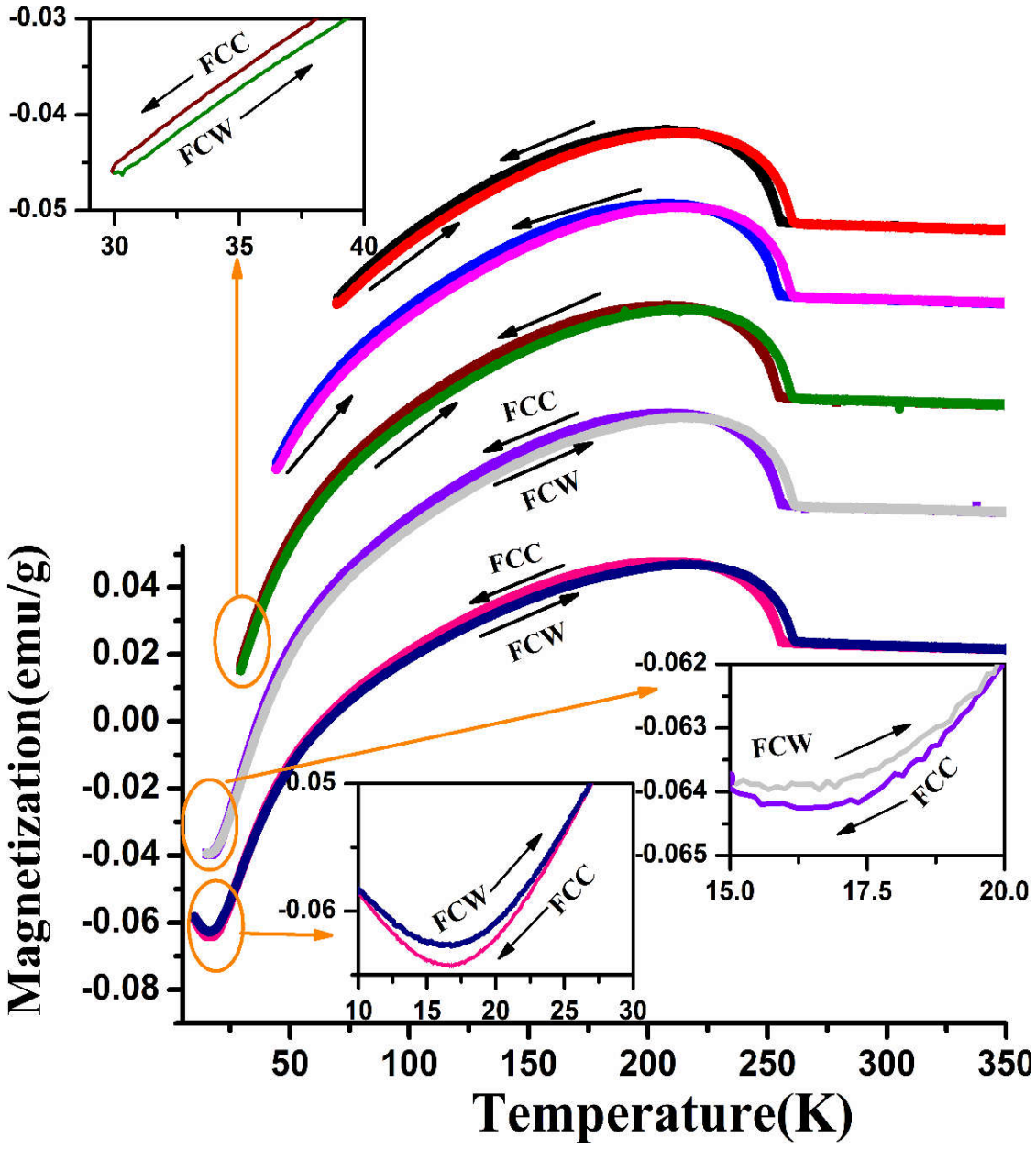

Figure 6.7 A sequence M vs. T curves under 500 Oe field, in FCC and FCW mode while turning back for FCW at decreasingly lower temperatures of 70,45,30,15 and 10K.

6.4.2 Field dependent magnetization

Figure.6.8 depicts magnetization as a function of applied magnetic field (±7 T) measured at 5, 20, 40, 60 and 210 K in ZFC mode. At each temperature, M vs. H shows a hysteresis loop with finite coercivity and remanent magnetization. Thus, we confirm that hysteresis is due to the spin canting of Cr^{3+}ions in $CeCrO_3$ like it is obvious in $GdCrO_3$, $TmCrO_3$ and $YbCrO_3$ materials [124,126,127].

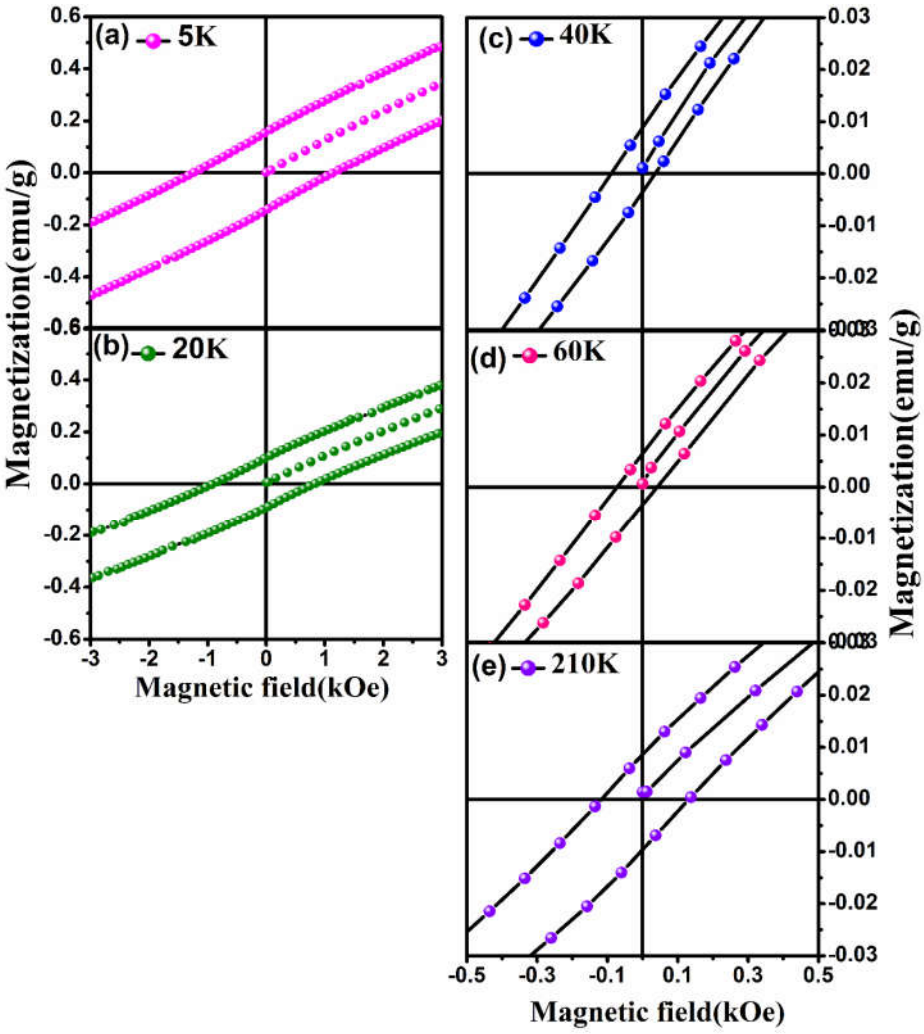

Figure 6.8 Isothermal magnetization curves, measured for $CeCrO_3$ in ZFC mode at 5, 20, 40, 60 and 210K.

It is further noticed that as the temperature decreases from 215K (T_{max}) to 58 K(T_{comp}), coercivity declines followed by a saturation down to 40 K. Below 40 K, coercivity again increases showing a maximum at 5 K. In $RCrO_3$, four magnetic ground state spin configurations such as $\Gamma_1(A_x,G_y,C_z)$, Γ_2 (F_x,C_y,G_z), Γ_3 (C_x,F_y,A_z) and $\Gamma_4(G_x,A_y,F_z)$are allowed. The $\Gamma_4(G_x,A_y,F_z)$ remains weakly ferromagnetic below T_N similar to the $LaCrO_3$ and $YCrO_3$ samples [49][133].When R ion is non-magnetic, the $\Gamma_4(G_x,A_y,F_z)$ persists throughout the temperature range of 2-300 K. When *R* is magnetic ion, not only $\Gamma_4(G_x,A_y,F_z)$ configuration but also $\Gamma_1(A_x,G_y,C_z)$ and $\Gamma_2(F_x,C_y,G_z)$ configurations are possible. Spin configuration, $\Gamma_1(A_x,G_y,C_z)$ does not allow any ferromagnetism hence no hysteresis whereas $\Gamma_2(F_x,C_y,G_z)$ configuration shows a weak ferromagnetism along *x* direction and presence of hysteresis [43]. It is also reported in $RCrO_3$ that coercivity for $\Gamma_2(F_x,C_y,G_z)$ spin configuration is higher compared to the $\Gamma_4(G_x,A_y,F_z)$ spin configuration [128]. As the coercivity at 5 K in $CeCrO_3$ nanoparticle is large compared to coercivity above T_{SR}, the possibility of transformation from $\Gamma_4(G_x,A_y,F_z)$ to $\Gamma_2(F_x,C_y,G_z)$ through continuous rotation of Cr^{3+}could be expected. Further, the irreversibility in M_{FCC} and M_{FCW} from magnetization vs. temperature measurement below T_{SR} supports the transformation from Γ_4 to Γ_2. Hence we conclude that, with decrease in temperature from 215 K Γ_4 spin configuration is transformed to Γ_2 below T_{SR} in these nano-particle. Further to explore exchange bias phenomena (H_E), M vs. H is measured at different temperatures with a measuring field range of ±70 kOe under the field cooling condition. Prior to each measurement, the sample is cooled down from 350 K to the desired temperature under a field of 10 kOe. Interestingly, the EB effect is observed in this system. The exchange bias, H_E is defined as $H_E = (H_1+H_2)/2$, where H_1 and H_2 are the right and left coercivity fields in the *M vs.H* curve. The field-cooled M vs. H curve at various temperature

are shown in figure 6.9. 8. Figure 6.10 depicts the temperature dependence of H_E. One may notice that NEB and PEB are observed at high temperature and at low temperature respectively.

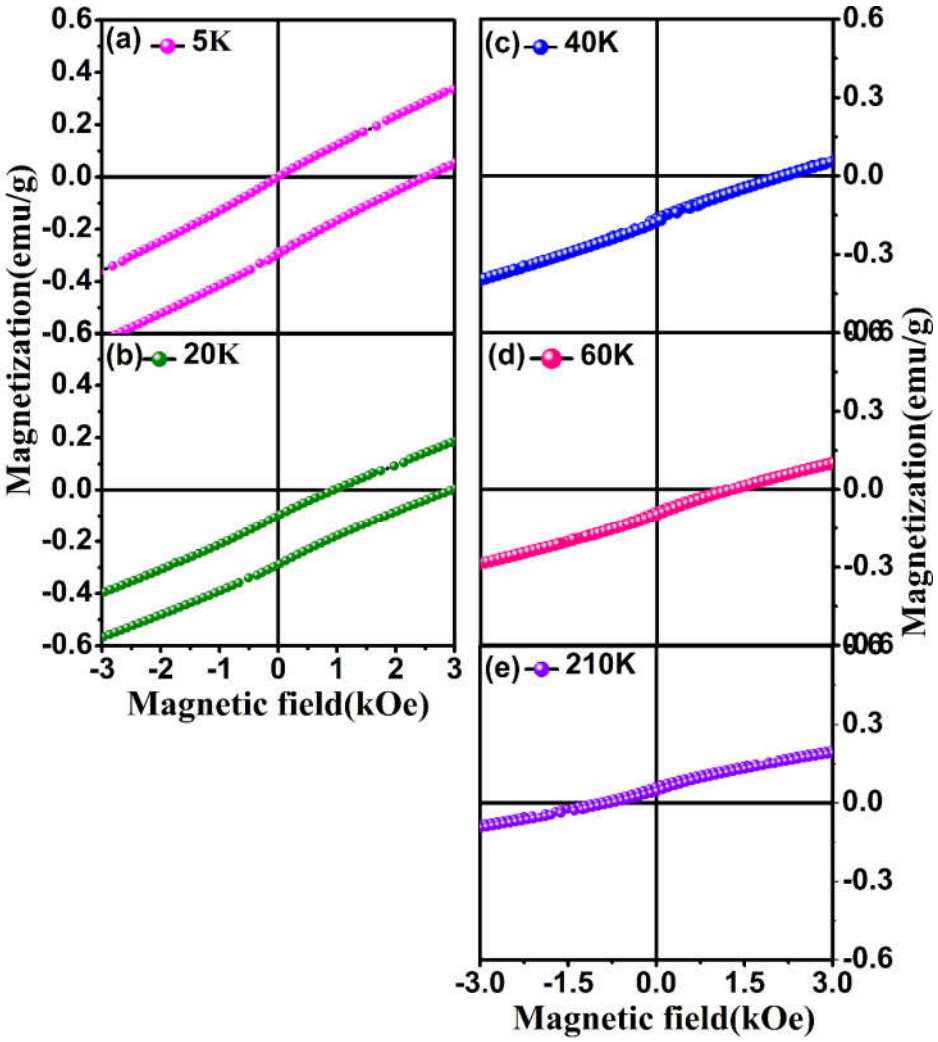

Figure 6.9 Isothermal magnetization curves, M vs. H, measured for $CeCrO_3$ in FC (@1T) mode at 5, 20, 40, 60 and 210K.

The highest positive exchange bias of 2.25 kOe is observed at around 40 K, while a minimum negative exchange bias of -1.25 kOe is detected at 210 K. Below 40K, the exchange bias is decreased to 1.25 kOe at 5 K, whereas above 40 K exchange bias decreases and shows

minimum exchange bias, -1.25 kOe at 210 K. It is clear from figure 6.10 that the exchange bias undergoes a transition from positive to negative around T_{cross} (110 K). The switching

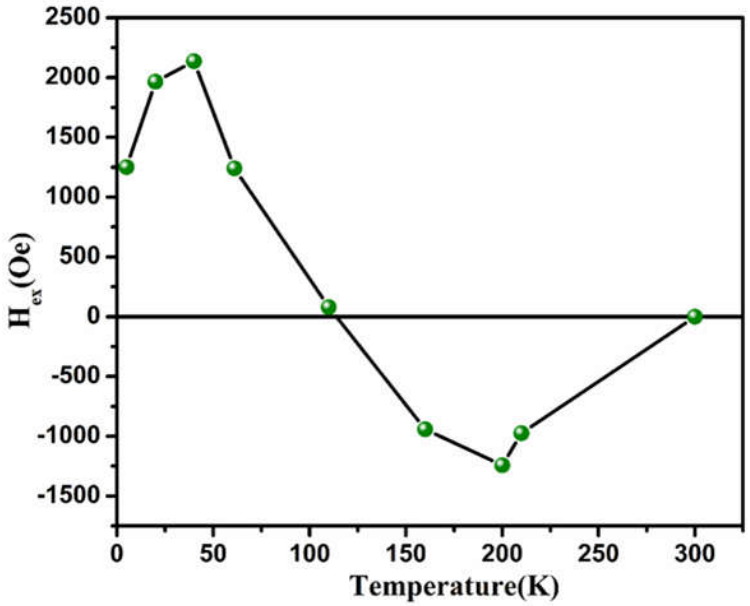

Figure 6.10 Exchange bias in MH at 5,20,40,60,110, 200 and 210K of $CeCrO_3$.

behavior of the exchange bias can be understood based on the antiferromagnetic interaction between Cr^{3+} and Ce^{3+} ions in $CeCrO_3$. Above T_{cross}, although Cr^{3+} and Ce^{3+}moments are antiferromagnetically coupled, Cr^{3+} moments dominate over Ce^{3+}. During the demagnetization process, the antiferromagnetic coupling hinders the reversal of Cr^{3+} moments, and hence requires an additional field to bring the magnetization closer to zero. As a result, the hysteresis loop shifts in the negative direction along the H axis and shows NEB. Below T_{cross}, the influence of Ce^{3+} moments become more prominent, especially below T_{comp}. In this regime, the Ce^{3+} moments align with the external applied field and become parallel to the direction of Cr^{3+} moments as the field increases. Therefore, the antiferromagnetic coupling between these moments supports the reversal of Ce^{3+} during the demagnetization process, leading to a smaller applied field in the negative direction required

to achieve zero magnetization. Consequently, the hysteresis shifts in the positive direction along the field axis and shows PEB. Similar kind of switching of exchange bias from positive to negative are also reported in $TmCrO_3$ and $YbCrO_3$ [126,127]. The switching of PEB to NEB with varying temperature is suitable for thermally assisted magnetic memory devices.

6.5 Conclusion

The nuclear and magnetic structure of $CeCrO_3$ synthesized through solution combustion method was presented. While temperature dependent nuclear structure demonstrated no structural change from 3-300K, magnetic structure analysis revealed the possible spin configurations such Γ_4, Γ_2 and Γ_1 which could not be distinguished due to small difference in lattice parameter between a and c, and strong coupling of moment along x and z direction. M vs. T measurement suggested the canted antiferromagnetic ordering of Cr^{3+}in $CeCrO_3$ just below T_N. Besides, an irreversibility in M_{FCC} and M_{FCW} showed the transformation of magnetic structure around T_{SR}. M vs. H measurement showed a weak ferromagnetic behavior with small H_C at 215K which indicated Γ_4 (G_x, A_y, F_z) magnetic structure. However, below T_{SR} the ferromagnetism with increased H_C indicated the Γ_2 (F_x, C_y, G_z) spin structure. Hence combining neutron diffraction with magnetization measurements confirmed the transformation of magnetic structure from Γ_4 to Γ_2 in $CeCrO_3$ nanoparticles. Further, sign reversal of EB driven by temperature was also detected. The elucidating of PEB and NEB was observed due to the competition between the AFM coupling of M_{Cr} and M_{Ce}. Such behavior is the main principle to design a thermally assisted magnetic random access memory (TAMRAM). Our new finding is expected to generate a considerable interest among the researchers working on spintronics devices.